Nonlinear and Transient Stability Analysis of Phase-Locked Loops in Grid-Connected Converters

Jiantao Zhao, Meng Huang, *Member, IEEE*, Han Yan, Chi K. Tse, and Xiaoming Zha, *Member, IEEE*

***Abstract*—The undesired nonlinear operation of phase-locked loops (PLL) is one of the main causes of transient instability in grid-connected converters. However, the stable operating region of PLL, knowing which is helpful for protection purposes, is hard to find due to the nonlinear characteristic of the transient process. In this article, the nonlinear characteristic of the PLL control loop relevant to the grid-connected converter operation is identified. The averaging method is applied to derive a time-domain expression for the PLL operation under disturbance. Based on the analytical expression, the transient response and related stability criterion are established, and the PLL design is improved while targeted to focus on various ac grid faults or disturbances. The results, applicable to transient stability enhancement, are verified by circuit simulations and experiments.**

***Index Terms*—Grid-connected converter, nonlinear analysis, phase-locked loop (PLL), transient stability.**

I. Introduction

As a consequence of rapid development of renewable power generation and high voltage dc transmission systems, more power electronics converters are deployed to serve as active interface with the ac power grid. However, unlike traditional synchronous machines with inherent high inertia, power electronics converters exhibit fast and complex transient processes under disturbances or fault conditions.

Inevitable system disturbances can be caused by the transmission line faults, large renewable source/power load swings, or frequency fluctuations, as reported in the US and in China [1]. In order to guarantee transient stability of the power electronics based power systems, high-capacity grid-connected converters should maintain synchronization with the power grid.

One of the key components in a grid-connected converter that is responsible for maintaining synchronization with the power system is the phase-locked loop (PLL) [2], [3]. With appropriate feedback control, the PLL maintains its stable operation and generates accurate frequency and phase references for the converter. However, under nonideal grid conditions, the behavior of the inherently nonlinear PLL becomes rather complex, posing possible stability issue to the converter that employs it [4].

The PLL is usually modeled together with the grid-connected converter. For instance, Wang *et al.* [5] established a unified impedance model and claimed that a high PLL bandwidth can be harmful to system stability in the face of system harmonic disturbances. Wen *et al.* [6] reported that a grid-tied inverter may be destabilized by the negative incremental resistor introduced by the PLL. This result was also extended to the multigrid converter system [7]. Much study has focused on stability assessment in terms of the passivity properties of the VSC input admittance [8], [9]. The state-space model is applied to the controller design of the grid-connected converter under weak grid conditions [10]–[12]. Studies were also conducted to analyze the effects of PLL using the transfer function approach. Excessive phase-loop bandwidth has been found to have an adverse effect on system stability [13]–[15]. Furthermore, a wide bandwidth or high proportional gain of the PLL has been shown to have a negative impact on the stability of the system [16]. However, setting a narrow PLL bandwidth to ensure stability of the converter may give unacceptable performance. Although a slow PLL and a fast voltage control loop may stabilize the converter in weak grid conditions, improper parameter settings may cause instability [10].

Most of the above studies use a simplified linear PLL model which cannot predict the complete instability characteristics of the system. Moreover, the nonlinear characteristic of PLL is quite critical, particularly in the transient process since the disturbances will cause significant shift on the system state. The mechanism of nonlinear oscillation in PLL has been analyzed, with due consideration of the nonlinearity of the phase detector in the analysis [17]. Also, the instability mechanism in the absence of a stable equilibrium point (SEP) has been analyzed using a quasi-static model in the frequency domain [18]. Han *et al.* [19] showed a transient process in which the PLL is directly destabilized by large disturbances of the grid side. The authors explained the instability based on the equal-area criterion (EAC) and derived the critical cleaning time for the converter. A similar phenomenon was also observed in the transient response of the wind turbine system subject to an ac grid fault [20]. Furthermore, Geng *et al.* [21] approximated the PLL as a synchronous generator, and analyzed the instability process of PLL using a method similar to that used in analyzing synchronous generator

Manuscript received January 25, 2020; revised April 2, 2020 and May 13, 2020; accepted May 26, 2020. Date of publication June 7, 2020; date of current version September 4, 2020. This work was supported in part by the National Natural Science Foundation of China under Grants 51637007 and 51877159, in part by the Hong Kong Research Grants Council under GRF 152096/17E, and in part by the Fundamental Research Funds for Central Universities Program under Grant 2042019kf0195. Recommended for publication by Associate Editor S. Golestan. *(Corresponding author: Meng Huang.)*

Jiantao Zhao, Meng Huang, Han Yan, and Xiaoming Zha are with the School of Electrical Engineering and Automation, Wuhan University, Wuhan 430072, China (e-mail: scarletzjt@whu.edu.cn; meng.huang@whu.edu.cn; han.yan@whu.edu.cn; xmzha@whu.edu.cn).

Chi K. Tse is with the Department of Electrical Engineering, City University of Hong Kong, Hong Kong (e-mail: chitse@cityu.edu.hk).

Color versions of one or more of the figures in this article are available online at https://ieeexplore.ieee.org.

Digital Object Identifier 10.1109/TPEL.2020.3000516

systems. On this basis, the EAC is used to explain the transient instability mechanism of the grid-connected converter with PLL. However, such applications of EAC cannot fully represent the control features of the PLL [22], [23]. Specifically, Wu *et al.* [23] proposed to use the phase portrait to predict the transient process and stability limit of the PLL, while He *et al.* [24] explained the instability process of the PLL and the resynchronization transient process by establishing a reduced order nonlinear model. The influence of the PLL's control parameters on the transient process has been analyzed qualitatively. Moreover, Bravo *et al.* [25] proposed to represent the nonlinear differential equation of the PLL as a dissipative Hamiltonian system and provided a better understanding of the PLL.

Although a great deal of effort has been devoted to study the nonlinearity of PLL, a nonlinear analytical model and stability criterion are still missing, which makes practical protection and antidisturbance design hard to realize.

To fill this research gap, this article is devoted to analyzing the nonlinear mechanism of PLL in grid-connected converters and deriving the analytical stability boundary. Therefore, the key contributions of this article are as follows.

1) The transient stability criteria of PLL are developed analytically. Using the averaging method, the transient solution of the PLL's nonlinear differential equation is obtained. The transient response of the PLL under disturbance including phase and magnitude jump, impedance, and current variations can be obtained in the time domain through this analytical solution.
2) The influences of various system parameters are studied. The grid impedance and initial phase angle have strong nonlinear effects on the PLL operation. Under weak grid conditions, the stability boundaries are developed considering these nonlinear effects.
3) A stability enhancement method is developed by limiting the phase output of the PLL. A saturation function is applied to the control loop of the PLL according to the analytical results. Although the transient adjustment time would be longer for the PLL, the transient stability can be guaranteed by this simple addition.

The rest of this article is organized as follows. In Section II, the nonlinear features of PLL in grid-connected converters are analyzed under various working conditions. In Section III, the analytical solution of the nonlinear dynamic equations of PLL is obtained by applying the averaging method. Based on the analytical solution, the transient stability criterion of PLL is derived. Section IV verifies the operating boundary with circuit simulations and experiments. Section V gives the conclusion.

II. Operation of PLL

Fig. 1 shows the grid-connected converter system. Under a weak grid condition, the grid side impedance cannot be ignored, as indicated by Z_s. Here, I_1, $I_{1\mathrm{ref}}$, and θ_1 represent the ac line current, the current reference, and the output phase angle of the PLL, respectively. Current control is applied in the inverter. The basic control diagram of the widely used synchronous reference frame PLL is shown in Fig. 2. The *dq* transformation

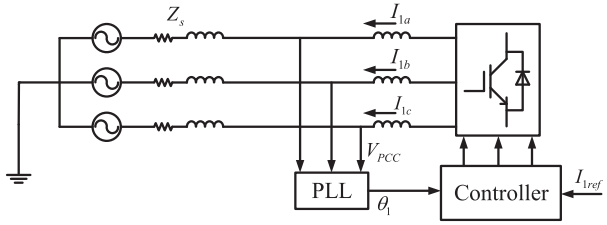

Fig. 1. Grid-connected inverter system schematic.

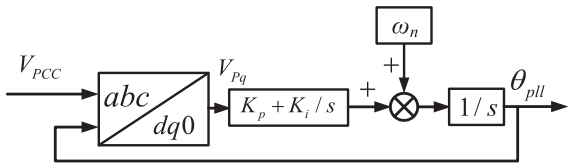

Fig. 2. SRF-PLL control block diagram.

TABLE I
System Parameters

Symbol	Description	Value
V_g (peak)	Grid voltage	155 V (1 p.u.)
f	System frequency	50 Hz (1 p.u.)
I_1 (peak)	AC current (before disturbance)	100 A (0.625 p.u.)
I_2 (peak)	AC current (after disturbance) set 1	160 A (1 p.u.)
I_3 (peak)	AC current (after disturbance) set 2	140 A (0.875 p.u.)
K_p, K_i	PLL control parameters of set 1	0.2,10
K_p, K_i	PLL control parameters of set 2	0.045,10
Z_s (R, L)	Grid impedance	3 mH (0.97 p.u.)
ξ_1	Damping ratio of set 1 (before/after disturbance)	0.32/0.07
ξ_2	Damping ratio of set 2 (before/after disturbance)	0.036/–0.01

allows the PLL to compare the ac voltage phase angle with the PLL output phase angle, and zero static control is achieved through a PI controller. The set of system and control parameters are listed in Table I. The grid voltage levels used in all subsequent scenarios in this article are the same as in Table I. Two simulation sets (set 1 and set 2) are used to represent different characteristics of the system. Detailed circuit simulation of a grid-connected converter system (inverter mode) is performed using MATLAB Simulink.

A. Unstable Transient Process

There are two kinds of unstable transient processes. As shown in set 1 simulation result given in Fig. 3, under large current disturbances (ac line current being stepped up to 160 A), the oscillation amplitude of the PLL crosses the unstable equilibrium point 1 (UEP1), causing the PLL to lose synchronization, as shown by red curve δ_{22}. This situation is similar to the conventional "first-swing angle instability" in the synchronous generator based power system, and can cause fatal failure in the grid-connected converter system.

However, in set 2 simulation, the blue curve δ_{21} shown in Fig. 3 indicates that under a *negative* damping condition,

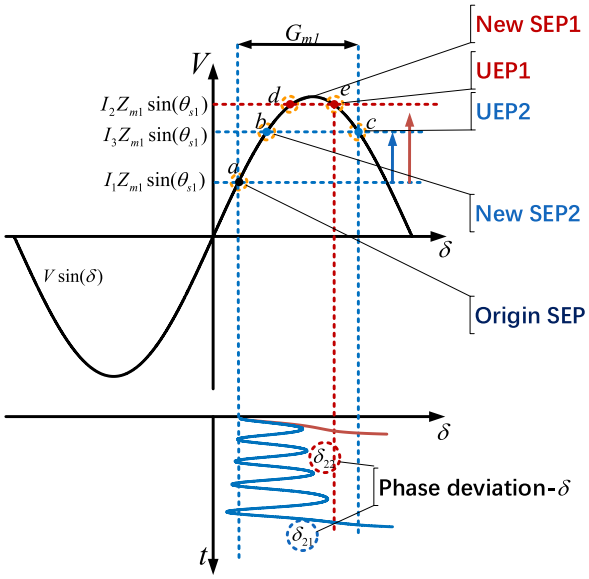

Fig. 3. Two unstable transient processes of PLL.

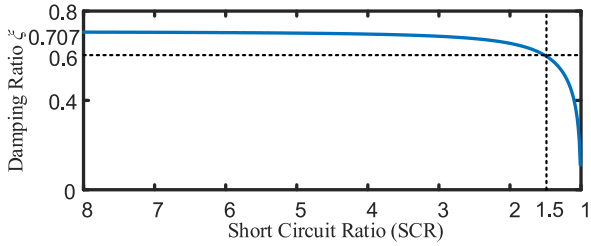

Fig. 4. Damping ratio of PLL system versus SCR, showing a rapid drop when SCR < 1.5. $K_p = 0.36$, $K_i = 10$, V_g(pk) $= 155$ V.

TABLE II
DAMPING RATIO UNDER DIFFERENT VALUES OF SCR

SCR	8	3	1.5	1.3	1.1
Damping Ratio (ξ)	0.707	0.687	0.600	0.544	0.403

corresponding to the control parameters K_p and K_i of set 2, a disturbance (ac line current being stepped up to 140 A) can cause the oscillation of the PLL to gradually diverge and lose synchronization after reaching UEP2. This corresponds to a "multiswing angle instability" in the system.

In order to describe the phenomena, we assume that the system operates at an SEP before the disturbance occurs, and assumes a new operating point after the disturbance occurs, and use the damping ratio of linear systems to describe the characteristic of the PLL. Different damping ratios are calculated for the two sets of simulation given in Table I.

In this article, changes in the point of common coupling (PCC) voltage are caused by changes in the grid-side impedance or changes in the line current. If an open circuit fault occurs in one of the double-circuit transmission lines, the grid-side impedance will increase, which will cause the PCC voltage to change and finally result in a phase angle shift. A three-phase short circuit or switching of large-capacity equipment could have the same effect.

B. Nonlinear Characteristic

Since the *dq* transformation is adopted to reveal phase detection, it can describe the nonlinear mechanism in the PLL. In the design of PLL and the analysis of small-signal stability of the converter, the sine function derived from the phase detector is normally equivalent to "1" in conventional linearization. Such equivalence is not applicable in weak grid conditions. Considering the nonlinearity of the phase detector, the PLL system under weak current network is linearized at each equilibrium point as a second-order system [27], which has a varying damping ratio given by

$$\xi = \frac{K_p k_{\sin} V_g - K_i I_1 (Z_s \varphi' \cos\varphi + Z'_s \sin\varphi)}{2\sqrt{1 - K_p I_1 (Z_s \varphi' \cos\varphi + Z'_s \sin\varphi)}\sqrt{K_i k_{\sin} V_g}} \quad (1)$$

where $k_{\sin}$ is the cosine value corresponding to the equilibrium point of the PLL and φ is the impedance angle.

The above damping ratio varies with the working conditions. As shown in Fig. 3, for simulation set 2, the occurrence of disturbance causes the PLL to move from the SEP "*a*" to a new SEP2 "*b*." However, the negative damping ratio (–0.01) makes the PLL oscillating and diverging. Moreover, when it reaches UEP2 "*c*," the system loses stability. In set 1 simulation, the disturbance causes the PLL to move from SEP "*a*" to SEP1 "*d*." Although the PLL will perform a damped (converging) oscillation at "*d*," it may also reach UEP2 "*e*," and then loses stability directly.

The short-circuit ratio (SCR) of the grid-connected system is affected by the converter capacity connected to the power grid, which can be expressed as

$$\mathrm{SCR} = V_g / I_n Z_s \quad (2)$$

where V_g is the phase voltage and I_n is the rated line current. The variation of damping with SCR is shown in Fig. 4.

Here is a specific example. The PLL control parameters K_p and K_i are 0.36 and 10, respectively. The grid impedance is 0.62 mH. Other circuit parameters are as given in Table I (before disturbance). The value of SCR is equal to 8. The system is a strong grid. The damping ratio of the PLL system can be calculated as 0.707 based on (1), as shown in Fig. 4. When the SCR drops to 1.5 and below, the system damping drops sharply. This is extremely detrimental to the stability of the PLL. The damping ratio values under decreasing SCR are listed in Table II.

Thus, when addressing the stability issue of the grid-connected systems under a disturbed transient process, more information is still needed, mainly in following two aspects:

1) Analytical solution of the transient process of the system after application of a particular disturbance.
2) Transient stability criterion with respect to different disturbance levels and system parameters.

Although the information is contained in the above set of nonlinear equations, a time-domain analytical solution is still

desirable for understanding the transient stability problem of the grid-connected system containing a PLL.

III. Transient Stability Analysis

In order to obtain the transition solution given a certain initial condition, we consider the basic expression of the PLL phase angle under weak grid conditions.

A. Dynamic Characteristic Equation

From Fig. 2, the output of the PLL through the PI controller can be expressed as (3)

$$\begin{aligned}\theta_1 &= \int \left(\omega_n + K_p V_{Pq} + K_i \int V_{Pq}\right) \\ &= \int \omega_n + \int \left(K_p V_{Pq} + K_i \int V_{Pq}\right) \\ &= \theta_{gn} + \int \left(K_p V_{Pq} + K_i \int V_{Pq}\right). \end{aligned} \tag{3}$$

The difference between the grid phase angle and the output phase angle of the PLL is given by

$$\delta = \theta_{gn} - \theta_{\text{pll}}. \tag{4}$$

The q-axis voltage at the PCC, denoted as V_{Pq}, can be expressed as

$$V_{Pq} = V_g \sin(\theta_g - \theta_{pll}) + I_1 Z_s \sin(\theta_s) \tag{5}$$

where θ_s is the impedance angle. Then, using (3) to (5), the dynamic characteristic equation of the PLL can be written as

$$\delta = \int \left(K_p + K_i \int\right)(I_1 Z_s \sin(\theta_s) - V_g \sin(\delta)). \tag{6}$$

Considering that the grid-side impedance is composed of resistance R_g and inductance L_g, (6) can be written as

$$\begin{aligned}\delta &= \int \left(K_p + K_i \int\right) \\ &\quad \times \left(I_1 \sqrt{(\omega L_g)^2 + R_g^2} \frac{\omega L}{\sqrt{(\omega L)_g^2 + R_g^2}} - V_g \sin(\delta)\right) \\ &= \int \left(K_p + K_i \int\right)(I_1 \omega L_g - V_g \sin(\delta)) \end{aligned} \tag{7}$$

which is valid only in the steady state. However, during the transient process, the frequency of the line current would not change immediately along with the PLL due to the control delay. Therefore, the influence of grid resistance cannot be completely eliminated, though it would not have significant impact in most practical scenarios. Meanwhile, the resistance component will increase the system damping. Thus, we only focus on the case of pure reactance as the worst case here.

The grid impedance can be found as

$$Z_s = \omega L_g = (\omega_n + \delta')L_g. \tag{8}$$

From (7) to (8), we get the nonlinear part $f(\delta, \delta')$ of the state equation of the PLL as follows [23]:

$$\begin{aligned}\delta'' = f(\delta, \delta') &= \frac{K_i}{1 - K_p I_1 L_g} \\ &\quad \times \left(I_1 \omega_n L_g + I_1 \delta' L_g - V_g \sin\delta - \frac{K_p V_g \cos\delta}{K_i}\delta'\right). \end{aligned} \tag{9}$$

It should be noted that (9) is valid only when the grid-connected inverter still generates active power after disturbance. In this case, the UEP and transient response of the PLL mainly depend on the grid inductance. The impact of grid resistance is relatively small. When the inverter generates reactive power to provide voltage support for the grid, the UEP and transient response at this time are mainly affected by the grid resistance [28]. The grid inductance will no longer limit the injected current amplitude of the inverter.

For brevity, we define the following parameters:

$$\begin{cases} a_1 = (1 - K_p I_1 L_g)/K_i \\ a_2 = I_1 \omega_n L_g \\ a_3 = I_1 L_g \\ a_4 = K_p V_g / K_i. \end{cases} \tag{10}$$

Thus, the dynamic characteristic equation of the PLL can be simplified as

$$\delta'' = f(\delta, \delta') = (a_2 + a_3\delta' - V_g \sin\delta - a_4\delta' \cos\delta)/a_1. \tag{11}$$

B. Analytical Solution With Active Power Output

In order to study the transient process of the PLL, an analytical solution in the time domain is required to predict the operating trajectory and stability boundary. It is noted that an independent variable is implicit in the first-order differential equation. Approximate solutions such as harmonic balance and equivalent linearization are not applicable to solve this equation due to the composite trigonometric functions. Here, we use the Taylor series to deal with the trigonometric functions in the differential equation. Taylor expansion allows the equation to be solved while retaining the original nonlinearity.

The averaging method from nonlinear oscillation theory is adopted in the PLL analysis [26]. This method uses a first-order approximation for a quasi-linear autonomous system in the form of

$$\ddot{x} + \omega_0^2 x = \varepsilon f(x, \dot{x}). \tag{12}$$

The original general solution can be expressed as

$$x = a\cos\varphi + \varepsilon x_1(a, \theta) + \varepsilon^2 x_2(a, \theta) + \cdots + \varepsilon^n x_n(a, \theta). \tag{13}$$

Here, $x_1(a, \theta)$ to $x_n(a, \theta)$ are not functions of time t, but are functions of a and θ. Moreover, a and θ are functions of time t. The averaging method is a first-order approximation of the real solution. The second and higher order terms of ε are ignored in getting the solution.

The purpose of the averaging method is to transform the equations of motion with displacements as unknown quantities

into standard equations with amplitudes and phases as unknown quantities. Since both amplitude and phase are periodic functions that slowly change with time, they can be replaced by the average value of the period. This method is therefore called the averaging method. Mathematically, the averaging method is an approximate solution evolved from the variation of parameters in differential equation theory [27]. The basic idea is to use the integral constant of the derived solution as a new independent variable to find the approximate solution of the basic equation.

It is assumed that the perturbed PLL has a new SEP δ_1, and the trigonometric function in (9) is expanded as a second-order Taylor series at δ_1. Then, δ_1 can be calculated with circuit parameters after the disturbance is applied, i.e.,

$$\delta_1 = \arcsin(I_1\omega_n L_g \sin(\varphi_z)/V_g) \tag{14}$$

where I_1, L_g, V_g, and φ_z are, respectively, the current, grid impedance, grid voltage, and impedance angle after application of disturbance. To simplify the expression, we define

$$\begin{cases} s_0 = \sin\delta_1 - \delta_1\cos\delta_1 - \frac{\delta^2{}_1\sin\delta_1}{2} \\ s_1 = \cos\delta_1 + \delta_1\sin\delta_1 \\ s_2 = -\frac{\sin\delta_1}{2} \\ c_0 = \cos\delta_1 + \delta_1\sin\delta_1 - \frac{\delta^2{}_1\cos\delta_1}{2} \\ c_1 = -\sin\delta_1 + \delta_1\cos\delta_1 \\ c_2 = -\frac{\cos\delta_1}{2}. \end{cases} \tag{15}$$

Using the coefficients of δ as shown in (15), (9) can be expressed as

$$\delta'' + {\omega_0}^2\delta = \varepsilon f(\delta,\delta') = -(d\delta^2 + (a + b\delta + c\delta^2)\delta' + f) \tag{16}$$

where the coefficients are

$$\begin{cases} \omega_0 = \sqrt{V_g s_1/a_1} \\ a = (a_4c_0 - a_3)/a_1 \\ b = a_4c_1/a_1 \\ c = a_4c_2/a_1 \\ d = V_g s_2/a_1 \\ f = (V_g s_0 - a_2)/a_1. \end{cases} \tag{17}$$

Now the dynamic characteristics of the PLL, as described by (16), have the same form as (12). If ε is equal to 0, the solution of this equation will be a simple harmonic oscillation which can be expressed by a trigonometric function with constant amplitude and phase angle θ. As ε is not zero, both A_1 and θ are time-varying. Meanwhile, the disturbance will cause the position of the PLL SEP to drift. There will be a constant term A_0 in the solution. As shown in Fig. 3, after the current steps up from I_1 to I_2, the SEP moves from point a to d. Thus, we assume that (9) has a solution of the following form:

$$\begin{cases} \delta = A_0 + A_1\cos(\omega_0 t + \phi) = A_0 + A_1\cos\phi \\ \delta' = -A_1\omega\sin\phi \end{cases} \tag{18}$$

where A_0 is equal to δ_1 as given in (14). Substituting (16) into (18), we get

$$\begin{aligned} f(A_0 + A_1\cos\phi, -A_1\omega_0\sin\phi) = -\Bigg[& dA_0^2 + \frac{1}{2}dA_1^2 \\ & + f + 2dA_0A_1\cos\phi + \Bigg(- a\omega_0A_1 - b\omega_0A_0A_1 \\ & - c\omega_0A_0^2A_1 - \frac{1}{4}c\omega_0A_1^3\Bigg)\sin\phi + \frac{1}{2}dA_1^2\cos 2\phi \\ & - \left(\frac{1}{2}b\omega_0A_1^2 + c\omega_0A_0A_1^2\right)\sin 2\phi - \frac{1}{4}c\omega_0A_1^3\sin 3\phi\Bigg]. \end{aligned} \tag{19}$$

Then, the derivatives of A_1 and θ can be solved as

$$A_1' = -\frac{1}{\omega_0 2\pi}\int_0^{2\pi} f(A_0 + A_1\cos\phi, -A_1\omega_0\sin\phi)\sin\phi d\phi \tag{20}$$

$$\theta' = -\frac{1}{A_1\omega_0 2\pi}\int_0^{2\pi} f(A_0 + A_1\cos\phi, -A_1\omega_0\sin\phi)\cos\phi d\phi. \tag{21}$$

Integrating both sides of (20) and (21) gives

$$A_1^2 = \frac{4m{A^2}_{10}e^{-mt}}{cA_{10} + 4m - c{A^2}_{10}e^{-mt}} \tag{22}$$

$$\theta = \frac{dA_0}{\omega_0}t + \theta_0 \tag{23}$$

where A_{10} is the initial value of A_1 and θ_0 is the initial value of θ. The expression of m is

$$m = cA_0^2 + a + bA_0. \tag{24}$$

The initial value of the solution (18) is

$$\begin{cases} \delta(0) = \delta_0 \\ \delta'(0) = 0 \end{cases} \tag{25}$$

where δ_0 is the SEP before disturbance, and can be calculated through (14) with parameters before disturbance. Substituting (25) into (18) yields

$$\begin{cases} A_{10} = \delta_0 - A_0 \\ \theta_0 = 0. \end{cases} \tag{26}$$

Substituting (26) into (22), the analytical expression of A_1 is

$$A_1 = -\sqrt{\frac{4m(\delta_0 - A_0)^2}{\frac{c(\delta_0 - A_0)^2 + 4m}{e^{-mt}} - c(\delta_0 - A_0)^2}}. \tag{27}$$

From (18), (23), and (27), the analytical expression of PLL dynamic characteristic differential equation can be derived as

$$\begin{aligned} \delta = & -\sqrt{\frac{4m(\delta_0 - A_0)^2e^{-mt}}{c(\delta_0 - A_0)^2 + 4m - c(\delta_0 - A_0)^2e^{-mt}}} \\ & \times\cos\left(\omega_0 t + \frac{dA_0}{\omega_0}t\right) + A_0. \end{aligned} \tag{28}$$

Based on the time-domain solution above, the transient process can thus be predicted accordingly for any given ac line current level, grid impedance, and control parameters. Then, the current limit design and protection can be easily performed for grid-connected converters.

C. Stability Boundary

At the critical damping point, the PLL output will exhibit oscillation. This kind of low-frequency oscillation may occur in

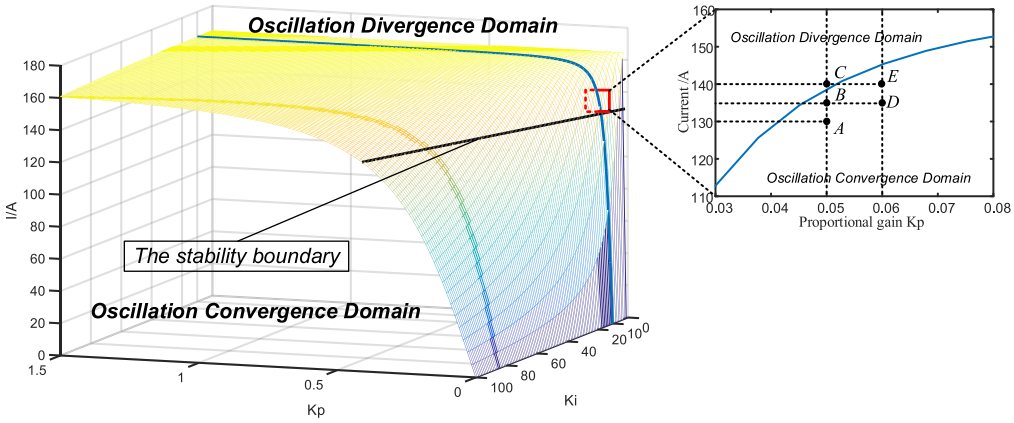

Fig. 5. Stability boundary surface in K_p-K_i-I space. Choosing values in the damped oscillation (convergence) domain can ensure system stability. If the disturbance causes a parameter to cross this boundary, the PLL will lose synchronization. Three operating points are marked in the figure on the right. Damping ratio: $\xi_{\mathrm{A}} = 0.014$, $\xi_{\mathrm{b}} = 0.006$, $\xi_{\mathrm{c}} = -0.002$, $\xi_{\mathrm{D}} = 0.021$, and $\xi_{\mathrm{E}} = 0.012$.

weak grid conditions. Therefore, a specific stability boundary is necessary to provide a reference for parameter design. When the PLL output oscillates with a constant amplitude, m is equal to zero, i.e.,

$$cA_0^2 + a + bA_0 = 0. \tag{29}$$

After substituting parameters and simplifying, the analytical expression of the stability boundary is

$$I_1 K_i L_g - K_p V_g \sqrt{1 - (I_1 Z_s \sin\phi / V_g)^2} = 0. \tag{30}$$

When $m = 0$, the output of the PLL will maintain a sustained oscillation. The amplitude of the oscillation AMP can be expressed as

$$\begin{aligned} \mathrm{AMP} &= \lim_{\substack{m\to 0 \\ t\to 0}} \sqrt{\frac{(\delta_0 - A_0)^2 e^{-mt}}{c(\delta_0 - A_0)^2(1 - e^{-mt})/4m + 1}} \\ &= \lim_{\substack{m\to 0 \\ t\to 0}} \sqrt{\frac{(\delta_0 - A_0)^2 e^{-mt}}{c(\delta_0 - A_0)^2 t + 1}} = \delta_0 - A_0. \end{aligned} \tag{31}$$

Based on the limitation given in (31), when the control parameters of the PLL are given, the circuit parameter values, including the injection current, the grid side impedance, and the grid side voltage, will vary within certain ranges. In this article, considering the variation of inverter output power and the possible ac faults, two sets of stability boundaries are given.

Fig. 5 shows the 3-D stability boundary in terms of the inverter injection current and the PLL control parameters under constant grid voltage and impedance values. They are the initial values in Table I. From the trend shown in the 3-D surface, it can be found that as the proportional gain of the PLL increases, the allowable injection current also increases. Moreover, the integral gain has an opposite effect on the stability.

When the system parameters are within the region below the stability boundary surface, that is, in the damped oscillation domain, the PLL can remain synchronization. If the line current value is raised beyond the stability boundary surface, the PLL output will oscillate and eventually lose synchronization.

Fig. 6 shows the 3-D stability boundary in terms of the grid side impedance and the PLL control parameters under constant grid voltage and injection current. The injection current is maintained at 130 A. At the stability boundary, the maximum grid side impedance value increases as the PLL's proportional gain increases, and decreases as the integral gain increases.

D. Analytical Solution With Reactive Power Output

Since (9) is not applicable to the grid-connected inverter when it generates reactive power, it is necessary to rederive the dynamic differential equation of the PLL. If the converter is designed to generate reactive current to provide voltage support during the voltage sag, the original dynamic characteristic equation should be modified as

$$\delta = \int \left(K_p + K_i \int \right) (I_1 Z_s \sin(\theta_s - \pi/2) - V_g \sin(\delta)). \tag{32}$$

The grid impedance Z_s consists of resistance R_g and inductance L_g. Similar to the derivation process in (7), based on the relationship between the grid impedance value and the impedance angle, (6) can be rewritten as

$$\delta = \int \left(K_p + K_i \int \right) (-I_1 R_g - V_g \sin(\delta)). \tag{33}$$

By differentiating both sides of (33), the dynamic equation of the PLL when the converter outputs reactive power can be obtained as

$$\delta'' = f(\delta, \delta') = -K_i I R_g - K_i V_g \sin\delta - K_p V_g \delta' \cos\delta. \tag{34}$$

Then, the analytical solution can be derived through the same process using the averaging method. To simplify the equation, we define

$$\begin{cases} n_1 = -K_p V_g \\ n_2 = -K_i I R_g \\ n_3 = -K_i V_g. \end{cases} \tag{35}$$

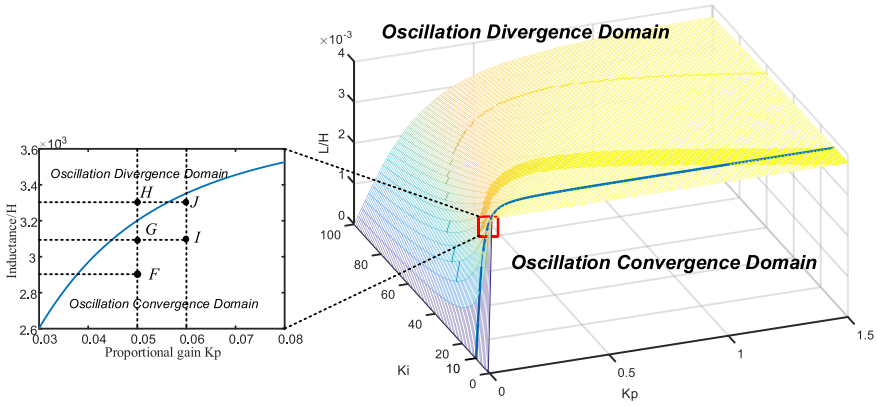

Fig. 6. Stability boundary surface in K_p-K_i-L space. Region below the boundary surface is the damped oscillation (convergence) domain, and the region above the boundary surface is the divergence domain. Three operating points are marked in the figure on the left. Damping ratio: $\xi_{\mathrm{F}} = 0.020$, $\xi_{\mathrm{G}} = 0.007$, $\xi_{\mathrm{H}} = -0.008$, $\xi_i = 0.022$, and $\xi_{\mathrm{J}} = 0.005$.

Thus, (34) can be written as

$$\delta'' = f(\delta, \delta') = n_1 \cos\delta + n_2 + n_3 \sin\delta. \tag{36}$$

The trigonometric functions are expanded into Taylor series near the new SEP δ_1. The coefficients in the Taylor series are the same as in (15). The calculation method of the SEP of the PLL when the inverter generates reactive power is different from that when the output power is active. At this time, the new SEP δ_1 of the PLL should be

$$\delta_1 = \arcsin(-I_1 R_g / V_g). \tag{37}$$

Then, substituting (15) into (36) yields

$$\delta'' + {\omega_0}^2\delta = \varepsilon f(\delta, \delta') = ((a + b\delta + c\delta^2)\delta' + d\delta^2 + f) \tag{38}$$

where

$$\begin{cases} \omega_0 = \sqrt{-n_3 s_1} \\ a = n_1 c_0 \\ b = n_1 c_1 \\ c = n_1 c_2 \\ d = n_3 s_2 \\ f = n_2 + n_3 s_0. \end{cases} \tag{39}$$

It is assumed that the solution takes the same form as (18). Using the same procedure, the amplitude and phase expressions of the solution are found as

$$A_1^2 = \frac{4mA_{10}^2 e^{mt}}{cA_{10} + 4m - cA_{10}^2 e^{mt}} \tag{40}$$

$$\theta = \frac{dA_0}{\omega_0} t + \theta_0. \tag{41}$$

The initial values of amplitude and phase are the same as when the inverter generates active power. By substituting (25), (40), and (41) into (18), a time-domain analytical solution of the PLL transient response when the inverter generates reactive power can be obtained as

$$\delta = \sqrt{\frac{4m(\delta_0 - A_0)^2 e^{mt}}{c(\delta_0 - A_0)^2 + 4m - c(\delta_0 - A_0)^2 e^{mt}}} \times \cos\left(\omega_0 t + \frac{dA_0}{\omega_0} t\right) + A_0. \tag{42}$$

Similar to the active power output case, the value of m determines the variation trend of the PLL output oscillation. The expression of m is

$$m = cA_0^2 + a + bA_0 = -K_p V_g \sqrt{\left(-I_1^2 R_g^2 + V_g^2\right)/V_g^2}. \tag{43}$$

Thus, it can be seen from (43) that as long as the proportional gain of the PLL is positive, the value of m will be negative. Thus, consistent with the result reported in [29], when the gain of the PLL controller is positive, the complex poles of the system will have negative real parts.

However, as stated above, the control delay will prevent the grid inductance from being completely eliminated during the transient process. Therefore, in order to avoid divergent oscillation, a larger proportional gain and a lower integral gain should be used.

IV. Verification

In order to verify the analytical solution obtained by the averaging method, several time-domain simulations are implemented in MATLAB Simulink with various levels of disturbance. The PLL control parameters in simulation A and B are $K_p = 0.05$ and $K_i = 10$. The initial grid voltage, line current, and grid impedance are 155 V, 130 A, and 3 mH, respectively.

A. Response of PLL With Four Types of Disturbances

The transient processes of PLL under four different types of disturbances are analyzed, including voltage and current magnitude jumps, phase angle jumps, and impedance variations, as shown in Fig. 7. In all simulations, the ac line current under the steady-state condition of the inverter is 130 A. In these simulations, the grid-connected converter generates active power during the transient process.

1) *Line current magnitude jump:* Fig. 7(a) shows the PLL response caused by the current jump. When the current jumps from 130 to 136.25 A, the oscillation gradually subsides as it has not yet crossed the stability boundary described in (26), as shown in the blue curve in Fig. 7(a). When the current jumps from 130 to 142.5 A, $m < 0$,

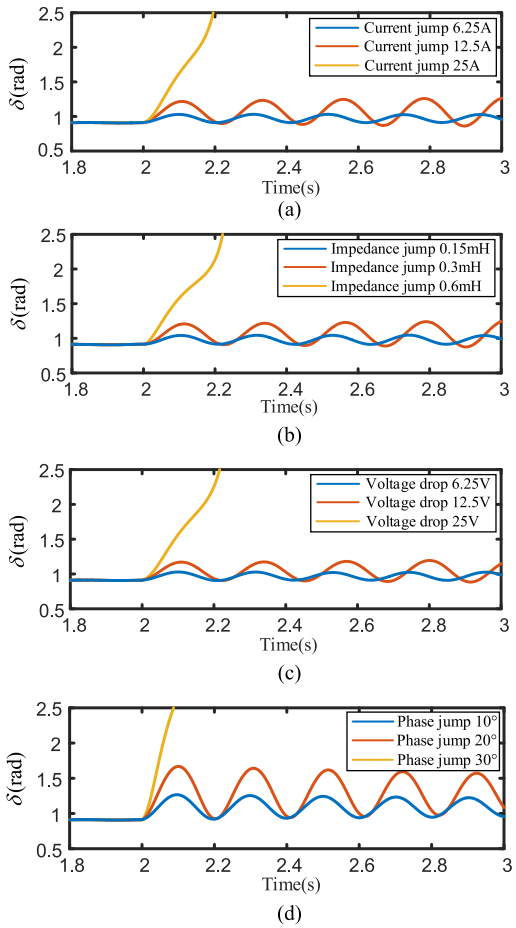

Fig. 7. Response of the PLL in four types of disturbance. At initial state $I_1 = 130$ A, $Z_s = 3$ mH, and $V_g = 155$ V. (a) Response of the PLL to current jump. (b) Response of the PLL to impedance jump. (c) Response of the PLL to voltage drop. (d) Response of the PLL to grid phase jump.

which means that the current value crosses the stability boundary. The output oscillation of the PLL diverges, as shown by the red curve. If the disturbance amplitude is further increased to 25 A, the phase angle deviation of the output of the PLL will exceed the UEP and results in instability. After crossing the UEP, even if the disturbance is cleared, the PLL can no longer recover stability, as shown by the yellow curve.

2) *Impedance variation:* Fig. 7(b) shows the response of the PLL caused by impedance change. The movement of SEP caused by impedance change is the same as the current jump. Similarly, the blue curve indicates that the impedance value has not yet crossed the stability boundary when the impedance jumps by 0.15 mH. The output oscillation of the PLL gradually subsides. The red curve indicates that when the disturbance amplitude is 0.3 mH, the impedance value exceeds the stable boundary and the oscillation diverges. The yellow curve indicates that the PLL loses stability under large disturbance.
3) *Grid voltage drop*: Fig. 7(c) shows the transient response process caused by the voltage drop. When the voltage drops by 6.25 V, the PLL can still return to a stable state. When the magnitude of the voltage dip increases to 12.5 V, the output oscillation of the PLL will diverge. When the voltage sag reaches 25 V, the output of the PLL directly exceeds the UEP.
4) *Grid phase jump:* Fig. 7(d) shows the PLL response caused by the grid phase angle jump. The variation of the phase angle does not cause the damping of the PLL to change. Therefore, as long as the PLL oscillation caused by the phase angle jump does not cross the UEP in the first cycle, the PLL can resume stability and reach a new operating point, as shown in the blue and red curves in Fig. 7(d). If the amplitude of the disturbance is further increased, the output of the PLL will exceed the UEP and lose synchronization, as shown by the yellow curve in Fig. 7(d).
5) From the above analysis, we see that the instability of the PLL can be examined under two cases. The first one is an oscillation with diverging amplitude caused by a certain parameter crossing the stability boundary, as shown by the red curve in Figs. 7(a)–(c). The other is caused by large disturbances, as shown by blue curve in Fig. 7.

For the type of instability where the system parameters cross the stability boundary, the control parameters can be optimized according to the stability boundaries to enhance transient stability.

B. Parameter Design Improvement

In Fig. 5, the stability boundary points corresponding to the current system simulation parameters are marked as red squares in the 3-D space. The K_p-I curve corresponding to this integral gain is marked in blue in the 3-D space. The operating points A, B, C, D, and E are marked in the enlarged view of the plane area near the oscillation boundary.

Fig. 8(a) shows the response of the PLL when the inverter's line current increases from I_{A} to I_{B}. The system damping ratio is reduced from 0.014 to 0.006, corresponding to points A and B in Fig. 5. The calculation yields $m > 0$, indicating that the output oscillation of the PLL should subside. It can be seen that both the output frequency and amplitude from the analytical solutions coincide with the simulation results. The convergence trend of the oscillation is also predicted by the calculation.

Fig. 8(b) shows the response of the PLL when the inverter's line current increases from I_{B} to I_{C}. The system damping ratio is reduced from 0.006 to –0.002, corresponding to points B and C in Fig. 5. The calculation yields $m < 0$, indicating that the output oscillation will diverge. The simulation result accurately verifies the analysis.

In order to avoid such divergent oscillation, the control parameters of the PLL can be designed according to the maximum disturbance amplitude and the stability boundary to ensure that the output oscillation of the PLL will not diverge after the disturbance.

Fig. 8(c) shows that the inverter's line current rising from I_{D} to I_{E}. The disturbance amplitude and operating point change are the same as those in Fig. 9(b). But the proportional gain of the PLL is increased to 0.06, corresponding to points D and E in

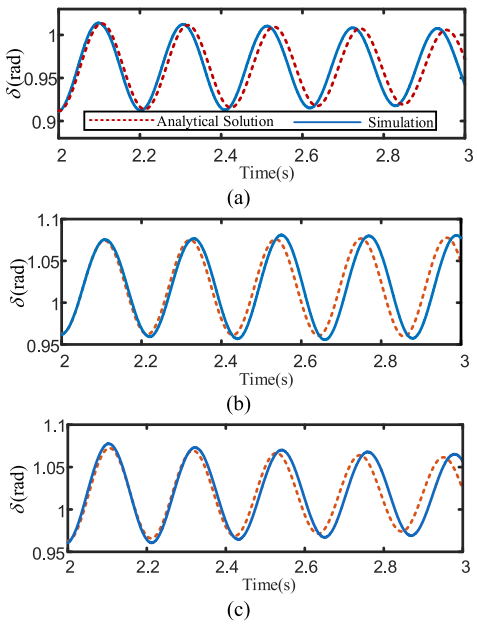

Fig. 8. Response of the PLL to output current. (a) A to B: Oscillation is damped as the operating point is within the boundary. (b) B to C: Oscillation diverges as the operating point crosses the stability boundary. (c) D to E: Oscillation converges as a more reasonable (larger) proportional gain K_p is set.

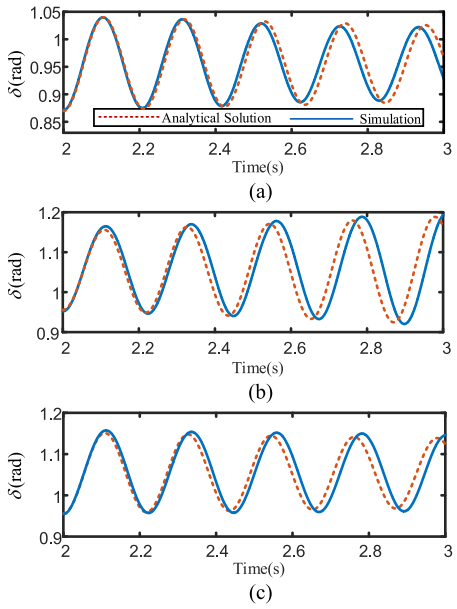

Fig. 9. Response of the PLL to grid impedance change. (a) F to G: Oscillation converges as the operating point is still below the boundary. (b) G to H: Oscillation diverges as the operating point crosses the stability boundary. (c) I to J: Oscillation converges as a more reasonable (larger) proportional gain K_p is set.

Fig. 5. After setting a larger proportional gain, the PLL can be stabilized after application of the disturbance.

The grid impedance may change due to the faults on the ac line. Three operating points are also marked in Fig. 6. As the operating point moves from F to G, the system remains stable, as shown in Fig. 9(a). However, when it moves from G to H, a diverging oscillation can be observed, as shown in Fig. 9(b). The converging/diverging trend of the oscillation is well predicted. In Fig. 9(c), the proportional gain is further increased. The operating point moves from I to J. Under the same disturbance as in Fig. 9(b), the output oscillation of the PLL can be damped.

In the above two cases, we only need to know whether or not the system converges to a new stable state. Therefore, the stability boundary can be easily established as the set of parameters for which a sustained oscillation occurs, as shown in Figs. 5 and 6.

TABLE III
SIMULATION PARAMETERS UNDER LVRT

Symbol	Description	Values
V_g (pk)	Grid voltage	155 V (1 p.u.)
f	System frequency	50 Hz (1 p.u.)
I_l (pk)	Line current	10 A (1 p.u.)
K_p, K_i	PLL control parameters	0.05,10
Z_s (R, L)	Grid impedance set2	0.3 Ω, 3 mH (0.02 p.u., 0.06 p.u.)

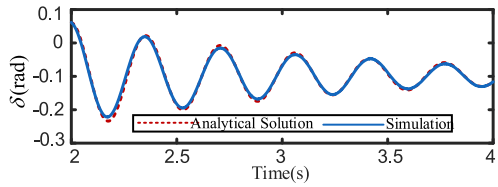

Fig. 10. PLL response when the converter in LVRT from 2 s.

C. Response of PLL During LVRT

The simulation results of the PLL response of the converter during the low voltage ride-through are shown in Fig. 9. The system parameters are shown in Table III. The grid impedance consists of resistance and inductance.

The grid voltage drops from 2 s to 0.2 p.u in the simulation. The inverter generates 1 p.u. of reactive current. If the inverter keeps generating active current, the value of m will be negative, giving a diverging oscillation of the PLL. This phenomenon does not occur because the inverter generates reactive power after disturbance.

Fig. 10 compares the simulation result and analytical solution when the injected current is 10 A (1 p.u.). It can be seen that the analytical solution agrees with the simulation result after the voltage drops at 2 s. The grid inductance has little impact during the transient process, and the differential equation (34) and its analytical solution (42) are still valid.

D. Accuracy of Averaging Method Under Large Disturbance

When the amplitude and period of the output of the PLL change by a large amount, the analytical solution and simulation result deviate significantly.

First of all, it should be pointed out that in such large disturbance cases, the analytical solution will deviate from the simulation. However, the displacement mainly depends on the amplitude of the disturbance (indicated by R in Figs. 11 and 12) and the position of the new SEP after the disturbance. The

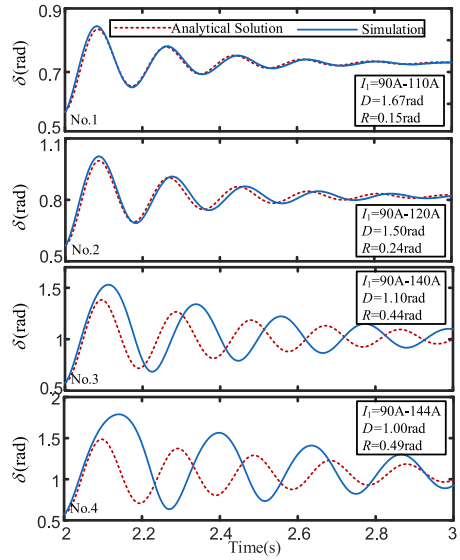

Fig. 11. Discrepancy between analytical solution and simulation result increases with the increase of the disturbance amplitude and the decrease of the distance between the SEP and the UEP. In simulation set 3 (third panel from top), when the injected current is increased from 90 to 140 A, significant amplitude and phase errors can be observed.

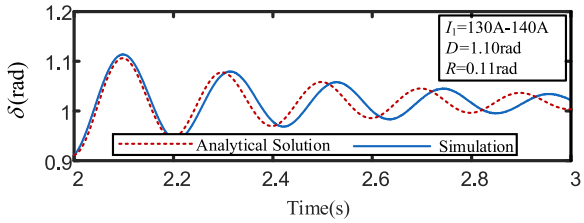

Fig. 12. Phase angle of PLL upon reducing the disturbance amplitude showing reduced error.

TABLE IV
SIMULATION PARAMETERS

Symbol	Description	Values
V_g(pk)	Grid voltage	155 V
f	System frequency	50 Hz
I_1 (pk)	Line current (before disturbance)	10 A/90 A/130 A
K_p, K_i	PLL control parameters of set 1	0.1,10
$Z_s(R,L)$	Grid impedance	3 mH

large disturbance amplitude produces output oscillation with rapid amplitude change. The amplitude of the disturbance can be expressed by the "distance" on the voltage-phase diagram between the original SEP and the new SEP of PLL.

Second, the new SEP after the disturbance determines the extent of nonlinearity of the PLL system. Short "distance" (indicated by D in Figs. 11 and 12) between the SEP and the UEP will give stronger nonlinearity of the system. These are the main reasons for the discrepancy between calculated and simulated results, and the trends of the difference are shown in Fig. 11. The system parameters used for this simulation are listed in Table IV.

As can be seen from Fig. 11, the error increases with the increase of disturbance amplitude. When the new steady-state operating point approaches the instability point (panels 3 and 4 in Fig. 11), the simulated oscillation waveform is no longer close to a sinusoidal waveform. The simulation waveform has severe distortion.

Fig. 12 is the comparison result of reducing the amplitude of the disturbance. It can be seen that after reducing the amplitude of the disturbance, the error in the analytical solution and the simulation results on the amplitude is significantly reduced, but there is still a certain phase error.

In addition, not all large perturbations would cause significant errors in the analytical solution. If the new SEP after the disturbance is kept away from the UEP, the simulation result and the analytical solution would still be consistent.

E. Experimental Verification

In Fig. 7, it is shown that under large disturbance, the phase angle deviation of the PLL δ will exceed the UEP. As a result, the PLL loses synchronization. This instability is irreversible. Due to the inherent nonlinearity of the PLL, the optimization method based on a linear model cannot ensure the transient stability of the PLL.

To ensure the stability of PLL in the transient process, a nonlinear method must be adopted. A common strategy in existing improvement measures is to detect the fault status and determine the required measures by calculation. This may require fast response speed and detection accuracy of the controller.

Protection can be adopted based on the principle of PLL instability and can be preconfigured according to the current working state of the PLL. Previous studies have shown that PLL loses synchronization when the phase angle deviation δ of the PLL exceeds the UEP. If the SEP of the PLL still exists after any disturbance occurs, there is a corresponding UEP. In order to avoid instability, we try to limit the amplitude of the output phase angle of the PLL. Using an output phase angle limiter, the PLL can gradually recover to a new stable state after the transient process if the SEP exists after the disturbance and the system parameters do not exceed the stability boundary. If the system parameters exceed the stability boundary after the disturbance or there is no SEP of the PLL during the transient process, the PLL will not enter an irreversible instability state as long as the output phase angle is limited. After the fault is cleared, the PLL can still return to the original stable state.

The transient behavior is verified in a practical weak grid-tied inverter of 2 kW, with the control implemented by the ARM-FPGA digital control platform, as shown in Fig. 13. The circuit and control parameters are listed in Table V.

In this case, the weak grid-connected inverter system would be unstable with the badly tuned PLL due to its poor damping effect. However, with proper controller protection limits, the inverter could be stable even under a large line current step-up. The transient response waveform is shown in Fig. 14.

When there is a line current step-up from 4 to 19 A (peak value), the inverter gets unstable. Large amount of harmonics

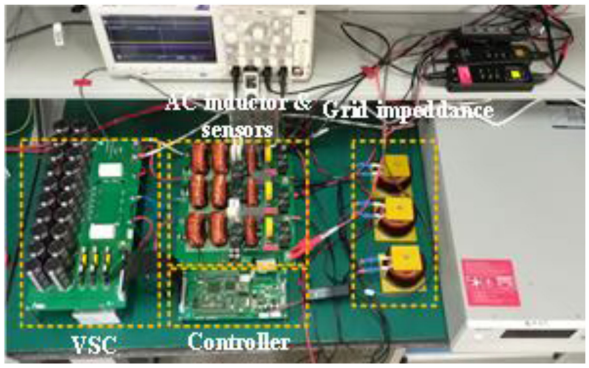

Fig. 13. 2-kW three-phase grid-connected converter prototype.

TABLE V
EXPERIMENTAL PARAMETERS

Symbol	Description	Values
V_g (peak)	Grid voltage	57 V
I_1 / I_2 (peak)	Line current before/after disturbance	4/19 A
L_g	Grid impedance	6.5 mH
Kp_{pll}	Proportional gain of PLL	0.001
Ki_{pll}	Integral gain of PLL	0.64
Limp	Proportional unit output limit	0.00015
Limi	Integral unit output limit	0.00015

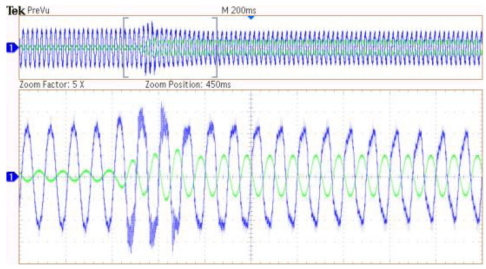

Fig. 14. Measured transient process of the inverter with proper PLL output limit. Blue waveform: PCC voltage V_g [25 V/div], cyan waveform: line current I_1 [20 A/div].

emerges at the PCC voltage. A significant phase error can be observed in the controller after this current disturbance. However, benefiting from the proper PLL output limits, the instability has been suppressed and the inverter enters a new stable operation point with higher line current and lower PCC voltage, as shown in Fig. 14. Therefore, the transient stability of the inverter can be enhanced by the PLL operation.

V. CONCLUSION

In this article, the nonlinear behavior of PLL in grid-connected converters is identified under various types of disturbance. Using the Taylor series to expand the trigonometric functions in the nonlinear dynamic equations, a simplified dynamic equation can be found based on the averaging method adopted from nonlinear oscillation theory. The different dynamic equations of PLLs corresponding to the grid-connected inverter generating active power and reactive power are derived. The stability boundary is found based on the analytical solution that covers various types of disturbance. An improved choice of control parameter, as guided by the stability boundary, can effectively enhance the tracking performance of the PLL in weak grid conditions. The transient solution is verified by circuit simulation of a grid-connected converter. It is shown that the system will lose stability after the disturbance due to the variation in damping, disturbance magnitude, and duration. In the control design, a stability enhancement method is developed by limiting the phase output of the PLL.

REFERENCES

[1] X. Xie, X. Zhang, H. Liu, H. Liu, Y. Li, and C. Zhang, "Characteristic analysis of subsynchronous resonance in practical wind farms connected to series-compensated transmissions," *IEEE Trans. Energy Convers*., vol. 32, no. 3, pp. 1117–1126, Sep. 2017.

[2] R. Teodorescu, M. Liserre, and P. Rodriguez, *Grid Converters for Photovoltaic and Wind Power Systems*. Hoboken, NJ, USA: Wiley, 2011.

[3] D. Xu, F. Blaabjerg, W. Chen, and N. Zhu, *Advanced Control of Doubly Fed Induction Generator for Wind Power Systems*. Hoboken, NJ, USA: Wiley, 2018.

[4] X. Wang, W. Du, and H. Wang, "Stability analysis of grid-tied VSC systems under weak connection conditions an overview," *Proc. Chin. Soc. Elect. Eng.*, vol. 37, pp. 1–12, Nov. 2017.

[5] X. Wang, L. Harnefors, and F. Blaabjerg, "Unified impedance model of grid-connected voltage-source converters," *IEEE Trans. Power Electron.*, vol. 33, no. 2, pp. 1775–1787, Feb. 2018

[6] B. Wen, D. Boroyevich, R. Burgos, P. Mattavelli, and Z. Shen, "Analysis of d-q small-signal impedance of grid-tied inverters," *IEEE Trans. Power Electron.*, vol. 31, no. 1, pp. 675–687, Jan. 2016.

[7] B. Wen, D. Dong, D. Boroyevich, R. Burgos, P. Mattavelli, and Z. Shen, "Impedance-based analysis of grid-synchronization stability for three-phase paralleled converters," *IEEE Trans. Power Electron.*, vol. 31, no. 1, pp. 26–38, Jan. 2016.

[8] R. Song, J. Guo, B. Li, P. Zhou, N. Du, and D. Yang, "Mechanism and characteristics of subsynchronous oscillation in direct-drive wind power generation system based on input-admittance analysis," *Proc. Chin. Soc. Elect. Eng.*, vol. 37, no. 16, pp. 4662–4670, Aug. 2017.

[9] L. Harnefors, L. Zhang, and M. Bongiorno, "Frequency-domain passivity-based current controller design," *IET Power Electron*., vol. 1, no. 4, pp. 455–465, Dec. 2008.

[10] M. F. M. Arani and Y. A. I. Mohamed, "Analysis and performance enhancement of vector-controlled VSC in HVDC links connected to very weak grids," *IEEE Trans. Power Syst.*, vol. 32, no. 1, pp. 684–693, Jan. 2017.

[11] A. Egea-Alvarez, S. Fekriasl, F. Hassan, and O. Gomis-Bellmunt, "Advanced vector control for voltage source converters connected to weak grids," *IEEE Trans. Power Syst.*, vol. 30, no. 6, pp. 3072–3081, Nov. 2015.

[12] J. Z. Zhou, H. Ding, S. Fan, Y. Zhang, and A. M. Gole, "Impact of short-circuit ratio and phase-locked-loop parameters on the small-signal behavior of a VSC-HVDC converter," *IEEE Trans. Power Del.*, vol. 29, no. 5, pp. 2287–2296, Oct. 2014.

[13] Y. Huang, X. Yuan, J. Hu, P. Zhou, and D. Wang, "DC-bus voltage control stability affected by AC-bus voltage control in VSCs connected to weak AC grids," *IEEE J. Emerg. Sel. Topics Power Electron.*, vol. 4, no. 2, pp. 445–458, Jun. 2016.

[14] J. Hu, B. Wang, W. Wang, H. Tang, Y. Chi, and Q. Hu, "Small signal dynamics of DFIG-based wind turbines during riding through symmetrical faults in weak AC grid," *IEEE Trans. Energy Convers.*, vol. 32, no. 2, pp. 720–730, Jun. 2017.

[15] Y. Huang, X. Yuan, J. Hu, and P. Zhou, "Modeling of VSC connected to weak grid for stability analysis of dc-link voltage control," *IEEE J. Emerg. Sel. Topics Power Electron.*, vol. 3, no. 4, pp. 1193–1204, Dec. 2015.

[16] L. Harnefors, X. Wang, A. G. Yepes, and F. Blaabjerg, "Passivity-based stability assessment of grid-connected VSCs—An overview," *IEEE J. Emerg. Sel. Topics Power Electron.*, vol. 4, no. 1, pp. 116–125, Mar. 2016.

[17] D. Dong, B. Wen, P. Mattavelli, D. Boroyevich, and Y. Xue, "Grid-synchronization modeling and its stability analysis for multi-paralleled three-phase inverter systems," in *Proc. IEEE Appl. Power Electron. Conf. Expo.*, 2013, pp. 439–446.
[18] D. Dong, B. Wen, D. Boroyevich, P. Mattavelli, and Y. Xue, "Analysis of phase-locked loop low-frequency stability in three-phase grid-connected power converters considering impedance interactions," *IEEE Trans. Ind. Electron.*, vol. 62, no. 1, pp. 310–321, Jan. 2015.
[19] G. Han, C. Zhang, and X. Cai, "Mechanism of frequency instability of full-scale wind turbines caused by grid short circuit fault and its control method," *Trans. China Electrotech. Soc.*, vol. 33, no. 10, pp. 2168–2174, May 2018.
[20] W. Tang, J. Hu, Y. Chang, and F. Liu, "Modeling of DFIG-based wind turbine for power system transient response analysis in rotor speed control timescale," *IEEE Trans. Power Syst.*, vol. 33, no. 6, pp. 6795–6805, Nov. 2018.
[21] H. Geng, L. Liu, and R. Li, "Synchronization and reactive current support of PMSG-based wind farm during severe grid fault," *IEEE Trans. Sustain. Energy*, vol. 9, no. 4, pp. 1596–1604, Oct. 2018.
[22] M. G. Taul, X. Wang, P. Davari, and F. Blaabjerg, "An overview of assessment methods for synchronization stability of grid-connected converters under severe symmetrical grid faults," *IEEE Trans. Power Electron.*, vol. 34, no. 10, pp. 9655–9670, Oct. 2019.
[23] H. Wu and X. Wang, "Design-oriented transient stability analysis of PLL-synchronized voltage-source converters," *IEEE Trans. Power Electron.*, vol. 35, no. 4, pp. 3573–3589, Apr. 2020.
[24] X. He, H. Geng, and S. Ma, "Transient stability analysis of grid-tied converters considering PLL's nonlinearity," *CPSS Trans. Power Electron. Appl.*, vol. 4, no. 1, pp. 40–49, Mar. 2019.
[25] M. Bravo, A. Garcés, O. D. Montoya, and C. R. Baier, "Nonlinear analysis for the three-phase PLL: A new look for a classical problem," in *Proc. IEEE Workshop Control Model. Power Electron.*, Padua, Italy, Jun. 2018, pp. 1–6.
[26] J. Sanders, F. Verhulst, and J. Murdock, *Averaging Methods in Nonlinear Dynamical Systems*. New York, NY, USA: Springer, 2007.
[27] J. Zhao, M. Huang, and X. Zha, "Nonlinear analysis of PLL damping characteristics in weak-grid-tied inverters," *IEEE Trans. Circuits Syst. II: Express Briefs*, to be published, doi: 10.1109/TCSII.2020.2978026.
[28] M. G. Taul, X. Wang, P. Davari, and F. Blaabjerg, "An efficient reduced-order model for studying synchronization stability of grid-following converters during grid faults," in *Proc. Workshop Control Model. Power Electron.*, Toronto, ON, Canada, 2019, pp. 1–7.
[29] M. G. Taul, X. Wang, P. Davari, and F. Blaabjerg, "Systematic approach for transient stability evaluation of grid-tied converters during power system faults," in *Proc. IEEE Energy Convers. Congr. Expo.*, Baltimore, MD, USA, 2019, pp. 5191–5198.

Jiantao Zhao received the B.S. degree in electrical engineering from the Hefei University of Technology, Hefei, China, in 2017. He is currently working toward the M.S. degree with the School of electrical engineering and automation, Wuhan University, Wuhan, China.

His research interests include nonlinear behavior and transient stability of power electronic converters.

Meng Huang (Member, IEEE) received the B.Eng. and M.Eng. degrees from the Huazhong University of Science and Technology, Wuhan, China, in 2006 and 2008, respectively, and the Ph.D. degree from the Hong Kong Polytechnic University, Hong Kong, in 2013.

He is currently an Associate Professor with the School of Electrical Engineering and Automation, Wuhan University, Wuhan, China. His research interests include nonlinear analysis of power converters and power electronics reliability.

Dr. Huang was the recipient of the best paper award of the IEEE TRANSACTIONS ON POWER ELECTRONICS, in 2016. He serves as the Guest Associate Editor for the IEEE JOURNAL OF EMERGING AND SELECTED TOPICS OF POWER ELECTRONICS, the IEEE JOURNAL OF EMERGING AND SELECTED TOPICS OF CIRCUITS AND SYSTEMS, and the Associate Editor for the IEEE ACCESS.

Han Yan was born in Bozhou, China, in 1995. She received the B.Eng. degree in electrical engineering in 2019 from Wuhan University, Wuhan, China, where she is currently working toward the M.Eng. degree.

Her research interests include the modeling and stability analysis of power electronics.

Chi K. Tse received the B.Eng. (first class hons.) and Ph.D. degrees from the University of Melbourne, Melbourne, VIC, Australia, in 1988 and 1991, respectively.

He is currently a Chair Professor of Electrical Engineering with the City University of Hong Kong, Hong Kong. Prior to joining City University in October 2019, he was with the Hong Kong Polytechnic University, Hong Kong, where he was the Head of the Department of Electronic and Information Engineering, from 2005 to 2012, and was a member of the University Council, from 2013 to 2015. His research interests include complex network applications, power electronics, and nonlinear systems.

Dr. Tse was the recipient of several research and invention awards, including IEEE TRANSACTIONS ON POWER ELECTRONICS Paper Prizes, Geneva International Invention Exhibition's Gold Medals, and Silicon Valley International Invention Festival's Grand Prize and Gold Medal. He serves and has served as Editor-in-Chief for the IEEE TRANSACTIONS ON CIRCUITS AND SYSTEMS II, the IEEE CIRCUITS AND SYSTEMS MAGAZINE, the IEICE Nonlinear Theory and Applications, as an Editor for the *International Journal of Circuit Theory and Applications*, and an Associate Editor for a few other IEEE journals. He has been appointed to IEEE Distinguished Lecturer, in 2005, 2010, and 2018, and to Honorary Professorship and Distinguished Fellowship by a few Australian, Canadian, and Chinese universities.

Xiaoming Zha (Member, IEEE) was born in Huaining, China, in 1967. He received B.S., M.S., and Ph.D. degrees in electrical engineering from Wuhan University, Wuhan, China, in 1989, 1992, and 2001, respectively.

He was a Postdoctoral Fellow with the University of Alberta, Edmonton, AB, Canada, from 2001 to 2003. He has been a Faculty Member with Wuhan University, since 1992, and became a Professor, in 2003. He is currently a Deputy Dean with the School of Electrical Engineering, Wuhan University, Wuhan, China. His research interests include power electronic converter, the application of power electronics in smart grid and renewable energy generation, the analysis and control of microgrid, the analysis and control of power quality, and frequency control of high-voltage high-power electric motors.